Effects of Non-radiative energy transfer processes on the visible upconversion in $ZrO_2:Yb^{3+}/Er^{3+}$ nanocrystals

O. Meza,* L.A. Díaz-Torres,* P. Salas,** E. De la Rosa,*, D. Solís*

* Centro de Investigaciones en Óptica A.C., León, Gto. 37150 México, ditlacio@cio.mx.
** Centro de Física Aplicada y Tecnología Avanzada, Universidad Nacional Autónoma de México, A.P. 1-1010, Querétaro, Qro. 76000, México, psalas@fata.unam.mx.

ABSTRACT

The luminescence dynamics of both near infrared (NIR) and visible (VIS) emission of Yb and Er in nanocrystalline ZrO2 is studied. It is found that upconversion emission is dominated by back transfer processes over direct Yb to Er energy transfer processes. A microscopic rate equation model was developed to fit both NIR and VIS fluorescence decay trends simultaneously, and to quantify the different interaction parameters responsible of the involved energy transfer processes. The microscopic model takes in to account the crystalline phase as well as the size of nanocrystals.

Keywords: Lifetime, Nanocrystals, Ytterbium, Erbium, Zirconium Oxide.

1 INTRODUCTION

Infrared-to-visible upconversion luminescence in nanocrystals has attracted considerable attention due its potential in applications as color displays and up-converted lasers [1-3]. In recent years many nanocrystalline materials have been proposed has efficient upconverters, among these, nanosized ZrO_2 has proven to be a best candidate for visible ligth generation. Many trivalent rare earths have been studied for Infrared-to-visible conversion [4]. Particularly, Erbium has been extensively studied in optical communications systems and Infrared-to-visible conversion processes [5]. The Er^{3+} ion has a relatively low absorption cross-section for the transitions in the near-infrared NIR region around 1000 nm [6]. Furthermore, the Yb^{3+} ion exhibits a higher absorption cross-section in this region and then, codoping with Yb^{3+} has proven to be a successful alternative for the upconversion process [7].

One of most important characteristics of a material is the fluorescence lifetime [8].The fluorescence lifetime is difficult to predict because of its dependence of several parameters, such as crystalline phase, material host, crystal size and codoping ions. There are many theoretical models explaining those observations, Forster was pioneer in this work, continued later by Dexter [9], Inokuti and Hirayama [10], whose main purpose was to estimate the rates for energy-transfer processes. In spite that those models have been successfully applied to several materials, these models have not improved to overcome an important fact and main assumption: All ions are subject to a sum of interactions over a continuous distribution of luminescence trap centers [11]. This is certainly not the case in crystalline medium, where the ions are distributed in specific positions in the host lattice. Therefore, interactions among ions present a discrete distribution and for nanocrystals this property becomes quite important. In this work we present the fluorescence characterization of Yb/Er codoped nanocrystalline ZrO_2 with dopant concentrations. An estimation of the upconversion parameters (red and green emission) and their corresponding efficiencies are calculated and discussed by solving the microscopic rate equations that govern the dymanics of the fluorescence decays subject to different Non-Radiative Energy Transfer processes among Yb and Er ions [12].

2 EXPERIMENTAL CHARACTERIZATIONS

Nanocrystals were prepared by using the sol-gel method. We synthesize four samples (1%)Yb/(1%)Er, (2%)Yb/(0.1%)Er , (2%)Yb/(0.2%)Er and (2%)Yb/(0.5%)Er. The samples were obtained using zirconium n-propoxide (ZP) 70% purity, erbium nitrate $(Er(NO)3)3 \cdot 5H_2O)$ and ytterbium chloride $(YbCl_3 \cdot 6H_2O)$ 99.99% purity as precursors. All samples were aged at 65 ºC for 15 ~ 18 h. Afterwards the samples were dried at 300 ºC for 2 h, dehydrated (stabilized) at 500 ºC for 2 h and annealed at 1000 ºC for 5 h applying increment ramps of temperature. A detailed explanation of sample preparation was reported elsewhere [13].

The crystalline structure of the samples was investigated by X-ray diffraction (XRD) using a SIEMENS D-500 equipment provided with a Cu tube with Kα radiation at 1.5405 Å, scanning in the 20º to 70º 2θ. The average particle sizes obtained from XRD patterns using the Scherer equation were between 60 and 80 nm. Crystalline structures were refined with the Rietveld technique by using DBWS-9411 and FULLPROF-V3.5d codes, peak profiles modeled with a pseudo-Voigt function contained average crystallite size as one of its characteristic parameters .Transmission electron microscopy (TEM) was performed

in JEM-2200FS transmission electron microscope with accelerating voltage of 200 kV.

For the photoluminescence (PL) characterization a CW semiconductor laser diode centered at 970 nm was used as a pump source. The fluorescence emission was analyzed with a monochromator Acton Pro 500i and a R955 photomultiplier tube (Hamamatsu) connected to a mode-locking amplifier SR860 (Stanford). Fluorescence lifetime was measured using an SR540 chopper (Stanford) with a monochromator and photomultiplier connected to a LeCroy digital Oscilloscope.

3 THEORETICAL MODEL

The microscopic origin for non-radiative energy transfer processes can be visualized as an interaction between an excited ion, the donor D, and another not excited ion, the acceptor A, with an absorption transition resonant with the de-excitation of the first one [12]. For simplicity we represent this process by $\left(D_{FS}^{IS} \rightarrow A_{ES}^{IS}\right)_{ji}$. This notation indicates the j-th donor ion D_j has a non radiative relaxation from an initial state IS to a final state FS, and the freed energy excites the i-th acceptor ion Ai from an initial state IS up to an excited state ES. The transfer probabilities are due to dipole-dipole, can be written as [14]

$$W\left(D_0^1 \rightarrow A_1^0\right)_{ji} = \frac{1}{\tau_{D_0^1}}\left(\frac{R_{06}\left(D_0^1 \rightarrow A_1^0\right)}{R_{D_iA_j}}\right)^6 \quad (1)$$

where $R_{0S}\left(D_0^1 \rightarrow A_1^0\right)$ defines the critical distance of the non radiative transfer. τ_{FS}^{IS} is the radiative lifetime of a donor relaxing radiatively from the initial state IS to a final state FS. $R_{D_iA_j}$ is the distance between the j-th Donor and the i-th Acceptor. In general it is assumed a crystalline host, and in consequence the D and A ions are uniformly distributed in the possible crystalline sites within the crystal lattice. To study the non radiative energy transfer from the Yb^{3+} ions to the Er^{3+} ions, we have to consider the donor ions (Yb^{3+}) are two level ions whereas the acceptors ions (Er^{3+}) are five level entities (see Figure 1). Such active ions will be uniformly distributed at the available crystallite sites within the nanocrystallite. N_D and N_A are the total number of active ions inside of the ZrO_2:Yb^{3+}/Er^{3+} nanocrystal. Under this assumption, we represent the probability of the j-th D ion to remain in its excited energy level n (n = 1) at time t by $P_{D_j}^n(t)$; and the probability of the i-th acceptor A to remain in its excited energy level m (m = 1, 2,…,5) at time t by $P_{A_j}^m(t)$. This means that we need to write N_D+5N_A ordinary differential equations (GETME):

$$\frac{dP_{D_i}^1}{dt} = -\frac{1}{\tau_{D_0^1}}P_{D_i}^1 - P_{D_i}^1\sum_{j=1}^{NA}W\left(D_0^1 \rightarrow A_2^0\right)_{ij}P_{A_j}^0 \quad (2a)$$
$$- P_{D_i}^1\sum_{j=1}^{NA}W\left(D_0^1 \rightarrow A_3^1\right)_{ij}P_{A_j}^1 - P_{D_i}^1\sum_{j=1}^{NA}W\left(D_0^1 \rightarrow A_4^2\right)_{ij}P_{A_j}^2$$

$$\frac{dP_{A_i}^1}{dt} = -\frac{1}{\tau_{A_0^1}}P_{A_i}^1 + \frac{1}{\tau_{A_1^2}}P_{A_i}^2 - P_{A_i}^1\sum_{j=1}^{ND}W\left(D_0^1 \rightarrow A_3^1\right)_{ij}P_{D_i}^1 \quad (2b)$$

$$\frac{dP_{A_i}^2}{dt} = -\frac{1}{\tau_{A_0^2}}P_{A_i}^2 - \frac{1}{\tau_{A_1^2}}P_{A_i}^2 + P_{A_i}^0\sum_{j=1}^{ND}W\left(D_0^1 \rightarrow A_2^0\right)_{ij}P_{D_i}^1 \quad (2c)$$
$$- P_{A_i}^2\sum_{j=1}^{ND}W\left(D_0^1 \rightarrow A_4^2\right)_{ij}P_{D_i}^1$$

$$\frac{dP_{A_i}^3}{dt} = -\frac{1}{\tau_{A_0^3}}P_{A_i}^3 + \frac{1}{\tau_{A_3^4}}P_{A_i}^4 + P_{A_i}^1\sum_{j=1}^{ND}W\left(D_0^1 \rightarrow A_3^1\right)_{ij}P_{D_i}^1 \quad (2d)$$

$$\frac{dP_{A_i}^4}{dt} = -\frac{1}{\tau_{A_0^4}}P_{A_i}^4 - \frac{1}{\tau_{A_3^4}}P_{A_i}^4 + P_{A_i}^2\sum_{j=1}^{ND}W\left(D_0^1 \rightarrow A_4^2\right)_{ij}P_{D_i}^1 \quad (2e)$$

Where $Yb(^2F_{5/2},^2F_{7/2}) \rightarrow Er(^4I_{15/2},^4I_{11/2})$, $Yb(^2F_{5/2},^2F_{7/2}) \rightarrow Er(^4I_{13/2},^4F_{9/2})$ and $Yb(^2F_{5/2},^2F_{7/2}) \rightarrow Er(^4I_{11/2}, {}^2H_{11/2}+{}^4S_{3/2})$ transition were denoted as $W\left(Yb_0^1 \rightarrow Er_2^0\right)$, $W\left(Yb_0^1 \rightarrow Er_3^1\right)$ and $W\left(Yb_0^1 \rightarrow Er_4^2\right)$, and $\tau\left(Yb_0^1\right)$ and $\tau\left(Er_0^{IS}\right)$ are the free ion lifetimes for Yb^{3+} and Er^{3+} respectively from the level IS to ground state, when no energy processes are present (see Table). And $1/\tau\left(Er_{ES}^{IS}\right)$ are the relaxation rates of the Er^{3+} ions from its upper state IS (Initial State) to the next lower (Final State) state FS=IS-1, for IS=4,3,2. These radiative relaxation rates were obtained from Judd-Ofelt calculation done with the reported Judd-Ofelt parameters reported in [15].

By solving GETME, we are able to predict at any time all the individual populations of all the excited states of all the active ions within the nanocrystallite. For this model the only free parameters are the $W\left(D_0^1 \rightarrow A_2^0\right)$, $W\left(D_0^1 \rightarrow A_3^1\right)$ and $W\left(D_0^1 \rightarrow A_4^2\right)$ parameters correspondents to direct energy transfer $Yb(^2F_{5/2},^2F_{7/2}) \rightarrow Er(^4I_{15/2}, {}^4I_{11/2})$ and to upconversion processes $Yb(^2F_{5/2},^2F_{7/2}) \rightarrow Er(^4I_{13/2}, {}^4F_{9/2})$ and $Yb(^2F_{5/2},^2F^{7/2}) \rightarrow Er(^4I_{11/2}, {}^2H_{11/2}\text{-}{}^4S_{3/2})$ respectively.

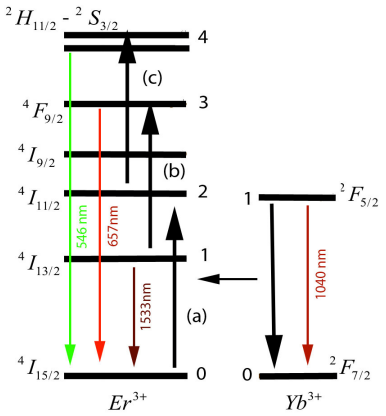

Figure 1: Energy levels diagram for the Yb^{3+}/Er^{3+} system. (a) direct energy transfer rate $Yb(^2F_{5/2},^2F_{7/2}) \rightarrow Er(^4I_{15/2},^4I_{11/2})$ and (c,b) upconversion processes $Yb(^2F_{5/2},^2F_{7/2}) \rightarrow Er(^4I_{13/2}, {}^4F_{9/2})$ and $Yb(^2F_{5/2},^2F_{7/2}) \rightarrow Er(^4I_{11/2}, {}^2H_{11/2}\text{-}{}^4S_{3/2})$.

Table 1: Free ion relaxation rates for ZrO2:Yb,Er

Transition	Value (s^{-1})	Transition	Value (s^{-1})
Yb ($^2F_{5/2} \rightarrow {}^2F7/2$)	1052.632	Er($^4F_{9/2} \rightarrow 4I15/2$)	1142.857
Er($^4I_{13/2} \rightarrow {}^4I15/2$)	147.058	Er($^4S_{3/2} \rightarrow {}^4I_{15/2}$)	1190.476
Er($^4I_{11/2} \rightarrow {}^4I15/2$)	86.956	Er($^4I_9/_2 \rightarrow 4I_{11}/2$)	12974.948
Er($^4I_{11/2} \rightarrow 4I13/2$)	58.719	Er($^4F_{9/2} \rightarrow 4I9/2$)	15986.433
Er($^4I_{9/2} \rightarrow 4I15/2$)	115.340	Er($^4S_{3/2} \rightarrow 4F9/2$)	14452.316

Sample	Critical distance (Å)		
Yb/Er%	$R(D_0^1 \rightarrow A_2^0)$	$R(D_0^1 \rightarrow A_3^1)$	$R(D_0^1 \rightarrow A_5^2)$
1/1%	6,010	5,996	5,996
2/0.1%	6,010	5,996	5,996
2/0.2%	10,575	8,929	5,913
2/0.5%	10,851	6,6118	7,951

The macroscopic normalized fluorescence emission of the excited state ES (ES=1..4) of species X (X= D or A) from an aggregate of k nanocrystallites is proportional to [12],

$$\varphi_X^{Es}(t;C) = \frac{\sum_{i=1}^{N_X} P_X^{Es}(t;C)}{N_X} \qquad (3)$$

Where $\varphi_X^{Es}(t;C)$ is a function of time (t) and dopant concentration (C), in order to solve the GETME by a 4th order Runge-Kutta numerical method, and then we use the Eq. $\varphi_X^{Es}(t;C) = \frac{\sum_{i=1}^{N_X} P_X^{Es}(t;C)}{N_X}$) for each excited level. To find $W(D_0^1 \rightarrow A_2^0)$, $W(D_0^1 \rightarrow A_3^1)$ and $W(D_0^1 \rightarrow A_4^2)$parameters we fit the experimental lifetime decay $\varphi_X^{Es}(t;C)$ with Eq. (3) for all dopant concentration for any time, that is to say the square difference between the model solution and experimental measurement for each dopant concentration (C), energy level (Es), ion type (X) and any time (t_i) need to be minimal:

$$f = \sum_C \sum_{Es} \sum_{X=A,D} \sum_{i=1}^{Nt} (\log \varphi_X^{Es}(t_i;C) - \log \Phi_X^{Es}(t_i;C))^2 \qquad (4)$$

To find minimum of constrained nonlinear multivariable function f we use the Trust-Region-Reflective Optimization method. [15].

4 RESULTS AND DISCUSSIONS

Figure 2 shows the VIS and NIR spectra emission integration as a function of dopant concentration. The Er($^4I_{13/2} \rightarrow {}^4I_{11/2}$), Yb($^2F_{5/2} \rightarrow {}^2F_{7/2}$), Er($^4F_{9/2} \rightarrow {}^4I_{15/2}$) and Er($^2H_{11/2}$-$^4S_{3/2} \rightarrow {}^4I_{15/2}$) emissions were observed among 1400-1620 nm, 1000-1100 nm, 640-690 nm and 510-580 nm respectively.

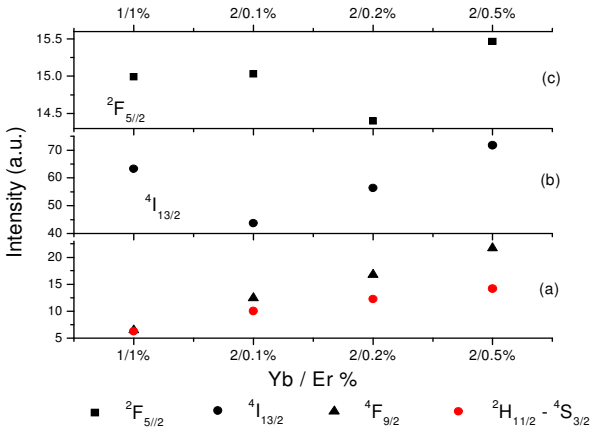

Figure 2. Emission intensity of ZrO2:Yb3+/Er3+ doped with Yb(1%),Er(1%), Yb(2%),Er(0.1%), Yb(2%),Er(0.2%) and Yb(2%),Er(0.5%).

The visible emission increases with the dopant concentration increment, nevertheless the red emission it is more intense than the green emission. The Er($^4I_{13/2} \rightarrow {}^4I_{11/2}$) emission for the same Yb concentration increases with the Er concentration increment. The Yb($^2F_{5/2} \rightarrow {}^2F_{7/2}$) emission does not show dependency with dopant concentration for the studied samples. Our simulations and experimental lifetime curves are shown in Figure 3. The effective lifetime [10] is obtained from the experimental fluorescence decay by the expression: $\tau_{eff} = \int I(t)dt / I(t=0)$. Our model, applied to all crystal samples, places the dopant ions randomly into the Zr sites of the lattice. With such a random placement of dopants, the total transfer rate is then calculated according to the assumed interaction (see eq. 1). Solving the eq. (4) for all samples, we estimate the critical distances (see table 1). This difference is due principally to the change of crystalline phase with dopant concentration. In addition we found that the Er($^4I_{11/2} \rightarrow {}^4I_{13/2}$) = (58.719 + 249.281) s^{-1} transfer rate is greater than that estimated by the Judd-Ofelt parameters. Then, the most probably is that increment is promoted partly by the phonon energy introduced by the presence of some impurities such as H_2O ($470cm^{-1}$). For most of the wet method synthesized nanocrystals there is always some contamination with high phonon energy centers, such as OH^- at 3400 cm^{-1} and CO^- at 1500 cm^{-1}, on the surface of nanocrystals, which can induce efficient nonradiative relaxation processes.

5 CONCLUSIONS

In summary, we have measured emission and lifetime curves of the fluorescence decay of Er(4I15/2), Yb($^2F_{5/2}$), Er(4F9/2) and Er($^2H_{11/2}$-$^4S_{3/2}$) energy levels in ZrO_2:Yb/Er. The crystalline phase of ZrO2: Yb3+, Er3+ nanophosphor is determined by the Yb^{3+} and Er^{3+} concentration and affected the emission properties of the nanocrystal.

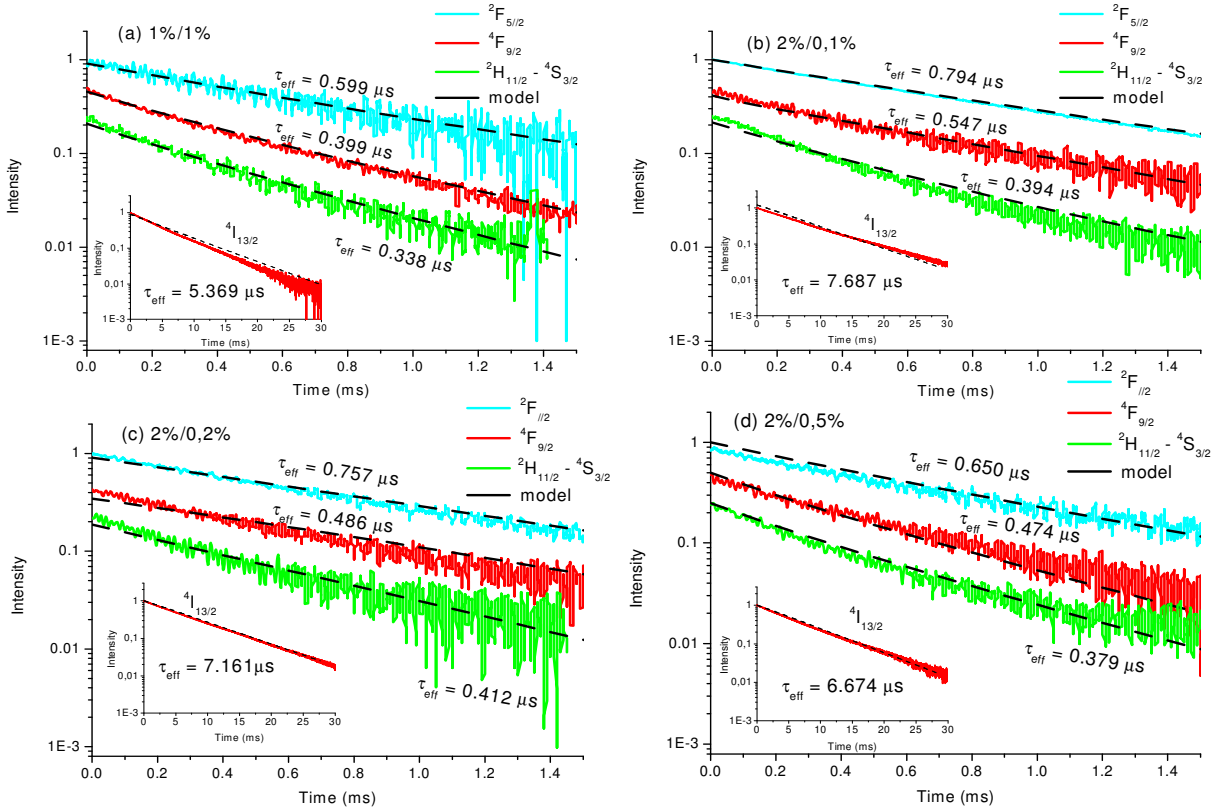

Figure 3: Experimental and simulated fluorescence decays of the ZrO_2:Yb,Er doped with (a) Yb(1%),Er(1%), (b) Yb(2%),Er(0.1%), (c) Yb(2%),Er(0.2%) and (d) Yb(2%),Er(0.5%).

The energy exchange between Yb^{3+} and Er^{3+} ions in the nanocrystal can be characterized by a dipole-dipole interaction. The critical distances depend of the dopant concentration due to the crystalline phase change. In addition the Er($^4I_{11/2} \rightarrow {}^4I_{13/2}$) transfer rate is greater than that estimated by the Judd-Ofelt parameters due to the action of impurities. Our interpretation is further supported by the application of solving General Energy Transfer Master Equations that govern the excitation dynamics of Yb and Er ions in a nanocrystal.

References

[1] H. Eilers, Materials Letters, 60 (2006) 214-217.

[2] R.N. Bhargava, J Lumin, 72-74 (1997) 46-48.

[3] A. Capobianco, F. Vetrone, T. D'Alesio, G. Tessari, A. Speghini, M. Bettinelli, Phys. Chem. Chem. Phys., 2 (2000) 3203-3207.

[4] G. Chen, G. Somesfalean, Y. Liu, Z. Zhang, Q. Sun, F. Wang, Physical Review B (Condensed Matter and Materials Physics), 75 (2007) 195204.

[5] D. Khoptyar, S. Sergeyev, B. Jaskorzynska, J. Opt. Soc. Am. B, 22 (2005) 582-590.

[6] E. Cantelar, J.A. Sanz-Garcia, F. Cusso, Journal of Crystal Growth, 205 (1999) 196-201.

[7] N. Yamada, S. Shionoya, T. Kushida, J. Phys. Soc. Jpn, 32 (1972) 1577-9.

[8] J.R. Lakowicz, Principles of Fluorescence Spectroscopy, Third Edition ed., Springer, 2006.

[9] D.L. Dexter, The Journal of Chemical Physics, 21 (1953) 836-850.

[10] M. Inokuti, F. Hirayama, The Journal of Chemical Physics, 43 (1965) 1978-1989.

[11] S.O. Vásquez, Physical Review B, 60 (1999) 8575.

[12] L.A. Díaz-Torres, O. Barbosa-García, C.W. Struck, R.A. McFarlane, J. Lumin, 78 (1998) 69-80.

[13] E. De la Rosa-Cruz, L.A. Diaz-Torres, R.A. Rodriguez-Rojas, M.A. Meneses-Nava , Appl. Phys. Lett, 83 (2003) 4903-4905.

[15] O. Meza, L.A. Diaz-Torres, P. Salas, E.D.l. Rosa, C. Angeles-Chavez, D. Solis, Journal of Nano Research, 5 (2009) 121-.130

[16] R.I. Merino, V.M. Orera, R. Cases, M.A. Chamarro, Journal of Physics, (1991) 8491.

[17] T.F. Coleman, Y. Li, An Interior Trust Region Approach for Nonlinear Minimization Subject to Bounds, in, Cornell University, 1993.